# A comprehensive study of the crystallization of Cu-As-Te glasses: microstructure and thermoelectric properties

Jean-Baptiste Vaney, Gaëlle Delaizir, Eric Alleno, Olivier Rouleau, Andrea Piarristeguy, Judith Monnier, Claude Godart, Michel Ribes, Raphael Escalier, Annie Pradel, et al.

# A comprehensive study of the crystallization of Cu-As-Te glasses: microstructure and thermoelectric properties

J. B. Vaney[1,2], G. Delaizir[3], E. Alleno[4], O. Rouleau[4], A. Piarristeguy[2], J. Monnier[4], C. Godart[4], M. Ribes[2], R. Escalier[2], A. Pradel[2*], A. P. Gonçalves[5], E. B. Lopes[5], G. J. Cuello[6], P. Ziolkowski[7], E. Müller[7], C. Candolfi[1], A. Dauscher[1], B. Lenoir[1]

[1]*Institut Jean Lamour (IJL), UMR 7198 CNRS-Université de Lorraine, France*

[2]*Institut Charles Gerhardt (ICG), UMR 5253 CNRS-Université Montpellier 2, France*

[3]*Sciences des Procédés Céramique et de Traitement de Surface (SPCTS), UMR CNRS 7315, Centre Européen de la Céramique, Limoges, France*

[4]*Institut de Chimie et des Matériaux de Paris Est (ICMPE), UMR 7182 CNRS, CMTR, Thiais, France*

[5]*ST/ITN Instituto Superior Técnico, Universidade Técnica de Lisboa, P-2686-953 Sacavém, Portugal*

[6]*Institut Laue Langevin, 6 rue Jules Horowitz, B. P. 156, 38042 Grenoble, France*

[7]*Institute of Materials Research, German Aerospace Center (DLR) Linder Hoehe, D-51147, Cologne, Germany*

## Abstract

We report a thorough experimental study on the microstructure, thermal behavior and thermoelectric properties of the amorphous composition $Cu_{15}As_{30}Te_{55}$ and the glass-ceramics related-compounds synthesized by Spark Plasma Sintering (SPS) technique. Varying the conditions of the SPS process enables the synthesis of composite glassy-crystalline samples with different crystal/glass ratios. Such treatments result in complex microstructures

composed of large glassy domains where nanocrystals of the metastable β-$As_2Te_3$ phase are embedded. These domains are separated by regions of dendritic crystalline phase surrounded by a Cu-rich glassy matrix. The presence of β-$As_2Te_3$, confirmed by both powder x-ray diffraction and scanning electron microscopy, suggests that pressure and/or internal stresses plays an important role in stabilizing this phase. This conclusion is further supported by neutron thermodiffraction experiments revealing a sharp crossover from the β-$As_2Te_3$ to the stable α-$As_2Te_3$ phase at temperatures below that of the SPS treatment. Transport properties measurements show that the presence of crystalline fraction significantly lowers the electrical resistivity by four orders of magnitude. However, the probable intrinsic *n*-type behavior of β-$As_2Te_3$ has a detrimental influence on the thermopower values. Even though the partial crystallization of the glassy matrix leads to an increase in the thermal conductivity, the measured values remain on the order of 1 $W.m^{-1}.K^{-1}$ at 300 K. Besides an overall increase in the dimensionless figure of merit *ZT*, our results demonstrate that the partial crystallization of an amorphous matrix is an efficient tool to tune the electrical resistivity over several orders of magnitude while maintaining low thermal conductivity values.

Keywords: glass-ceramics, chalcogenide, thermoelectric properties

*Corresponding authors: annie.pradel@univ-montp2.fr

## 1. Introduction

Thermoelectric materials offer an effective way to convert thermal energy into electrical energy (Seebeck effect) and, reciprocally, electrical energy into thermal energy (Peltier effect). The performance of thermoelectric devices is directly related to the materials' dimensionless thermoelectric figure of merit $ZT$ defined by $ZT = \frac{\alpha^2 T}{\rho\lambda} = \frac{PT}{\lambda}$ where $T$ is the absolute temperature, α is the Seebeck coefficient (or thermopower), $P = \alpha^2 / \rho$ is the power factor, $\rho$ is the electrical resistivity and $\lambda$ is the total thermal conductivity.[1]

A good thermoelectric material should display simultaneously a large thermopower, a low electrical resistivity and a low thermal conductivity. However, these three transport properties are mutually interdependent via the carrier concentration, making the optimization of the thermoelectric properties a complex task. In most thermoelectric materials, optimum power factors are obtained when the carrier concentration ranges between $10^{18}$ and $10^{21}$ $cm^{-3}$ at room temperature *i.e.* in heavily doped crystalline semiconductors or semimetals.[2,3] Another key ingredient leading to high thermoelectric materials is their complex crystalline structure that enables to lower the thermal conductivity values. Several strategies are usually employed to disrupt more efficiently the heat-carrying acoustic phonons either on an atomic or a microscopic scale. The former possibilities include mass fluctuations upon alloying or the presence of loosely-bounded atoms in oversized atomic cages.[3] Nanostructuring is at the heart of the latter approach through a combination of a micron-sized matrix embedding nanoscale precipitates across multiple length scales.[4-7]

A radically different strategy may be adopted by focusing on materials exhibiting intrinsically very low thermal conductivity values leaving $P$ the only relevant parameter to be optimized. Organic amorphous materials like conducting polymers have been attracting great

attentions in recent years for their promising thermoelectric properties around room temperature.[8-10] Inorganic glassy materials offer also this possibility since their ability to conduct heat is hampered by their inherent disorder. In addition, the plethora of chemical compositions achievable allows tuning their electronic properties from metallic-like to semiconducting-like, for instance, in glasses based on chalcogenides (S, Se, Te) and/or pnictides (As, Sb, Bi, etc).[11] However, one of the main obstacles to consider them for thermoelectric applications is their high electrical resistivity, which has prevented so far to achieve large *ZT* values.

A fine control of the electrical resistivity therefore appears as the most challenging problem to be overcome before further considering these materials as potential thermoelectric materials. Though a first possibility would consist in varying the compositions to control the carrier concentration as in their crystalline analogues, a precise knowledge of the exact coordination number of the atoms is difficult to achieve. Another strategy relies on a controlled partial crystallization of the glassy matrix to lower the electrical resistivity. Provided a precise control of the fraction of crystalline phase can be obtained, this innovative approach might help to improve the thermoelectric properties and hence, warrants further attention.

Here, we report detailed investigations on semiconducting chalcogenide glasses and glass-ceramics based on the Cu-As-Te system. More precisely, we focused on the glass composition $Cu_{15}As_{30}Te_{55}$ and studied the influence of the crystalline nature and fraction on its thermoelectric properties. The choice of this particular composition is based on two main characteristics suitable for the purpose of the present study. First, the synthesis of a pure amorphous form of this compound can be easily done by a conventional quenching method and thus, does not need ultrafast-quenching techniques such as melt-spinning. Second, this glass composition has a very high electrical resistivity with respect to glasses containing

higher Cu contents so that the influence of a crystallized fraction on ρ is expected to be exacerbated.

## 2. Experimental

The glassy samples were synthesized in silica tubes under secondary vacuum. Starting elements, As (Goodfellow, 99.99%), Te (5N+, 99.99%) and Cu (Sigma-Aldrich, 99.999%), were first weighed in stoichiometric quantities (to obtain a total batch of ~ 5g) and introduced in a silica tube. The tube was subsequently evacuated, sealed and heated in a furnace with the low heating rate of $9K.h^{-1}$ up to 1123K, held at this temperature for 2h and eventually quenched in a salt-ice-water mixture. The resulting ingots were hand-ground to micron-sized powders.

The thermal behavior of the as-quenched samples were studied by Differential Scanning Calorimetry (DSC) performed using TA instrument Q100 equipment from room temperature up to 573K using different heating rates ranging from 5 up to $40K.min^{-1}$.

Spark Plasma Sintering (SPS) of the powders was realized with the Dr. Sinter 505 Syntex, the set-up belonging to the "Plate-forme de Frittage Ile de France" (Thiais, France). This technique allowed us to obtain both amorphous bulk samples as well as glass-ceramic composites. The amorphous powders were introduced in a 8mm diameter graphite die. To gain further insights into the influence of this process on the crystalline fraction, we varied the dwell time parameter from 0 to 30 minutes at a temperature of 423K or 433K and under a pressure of either 50MPa or 100MPa.

The density of the different glass and glass-ceramics bulk was determined through the Archimedean principle using a Kern balance. This balance enables weighing solids in air ($m_{air}$) as well as in a solvent (in our case, water $m_{water}$). If the density of the buoyancy medium is known ($\rho_0$) the density of the solid ($\rho$) is calculated as follows:

$$\rho = \frac{m_{air}}{m_{air} - m_{water}} \rho_0 \quad (1)$$

The microstructure of both the amorphous and glass-ceramics bulk samples was investigated on fresh fracture along the cross section using a LEO SEM-FEG microscope. Composition of crystalline and glassy phases was estimated using Energy Dispersive X-ray Spectroscopy (EDXS) on a polished cross-section surface.

To identify the crystalline phases, powder x-ray diffraction (PXRD) measurements on the surface of the SPS bulk samples were carried out at room temperature using a D8 Bruker diffractometer equipped with a Vantec 1D-detector. To derive the integral breadth of the x-ray line of the crystalline phase, a pattern was recorded in the 2θ range 10-90° with another D8 diffractometer equipped with a 1D-detector and a primary monochromator filtering the Cu-$K\alpha_2$ emission line. A good signal-to-noise ratio at large 2θ was obtained for a total recording time of 96 hours. The integral breadths of several lines were determined by fitting a Lorentzian profile on a background-subtracted pattern. The instrumental contribution to the integral breadth ($\beta_i$) was determined by a preliminary experiment on $LaB_6$ and subtracted from the observed integral breadth ($\beta_0$) to provide an estimated intrinsic sample broadening ($\beta_e$).

Neutron thermodiffraction was used to study the crystallization process occurring in the glasses upon heating. The neutron diffraction experiments were performed using the D1B instrument at the Institut Laue–Langevin in Grenoble (France) with a nominal wavelength of 2.52Å. Two samples of compositions $Cu_{15}As_{30}Te_{55}$ and $Cu_{20}As_{20}Te_{60}$ were placed in non-sealed cylindrical vanadium containers in vacuum (outer diameter of 8mm and inner diameter of 7.6mm). Using a standard ILL furnace (vertical top loading furnace), neutron diffraction spectra were continuously collected on samples subjected to the following heating ramps: from room temperature to 363K at a rate of 5K/min and then from 363K to 473K at a lower

rate of 0.1K/min. For the cooling process, the furnace was simply switched off to allow the samples to reach room temperature in 'free fall'.

Electrical resistivity measurements were performed on disk-shaped samples (Ø ~ 8mm) using the van der Pauw technique.[12] The disks were then cut in bar-shaped samples (~ $1\times1\times8mm^3$) for thermopower measurements performed under argon atmosphere between 300K and 360K. The measurements were done at fixed temperatures using a homemade apparatus based on the differential method.[13] Stabilized positive and negative thermal gradients ($\Delta T$ ~ 2K) were applied by heating alternatively each end of the sample: the thermopower values were then obtained as an average of the forward and reverse values. The temperature gradient and thermoelectric voltage were measured by two *n*-type thermocouples pressed by mulite rods against one side of the sample.

Thermopower mapping was conducted under vacuum using a potential Seebeck microprobe (PSM) on a sample surface of $4\times0.5mm^2$ with a resolution of $10\times10\mu m^2$.[14] This measurement was performed on a glass-ceramic sample obtained at 423K, 50MPa, 30min. dwell time. The scan direction of the measurements was in rising *x*-direction (type writer style), beginning from zero for every new line. The contact detection was established by a load cell and a microcontroller giving a trigger signal to the transient recorder. The applied force at each measurement point was about 1.65 $mN/\mu m^2$. The elapsed time between contact and desired force-trigger was about 3 ms. For each point, two thermopower values were saved from different time domains. The measurement temperature is estimated to be 5 to 10 K above room temperature. Black fragments visible in the resulting maps along the measurement direction or as a single point are due to contact problems.

The thermal conductivity was determined at room temperature via thermal diffusivity measurements performed under argon atmosphere on cylinder-shaped samples using a LFA 427 (Netzsch) equipment. Both properties are related by the formula $\lambda = aC_p\rho_V$ where $a$ is

the thermal diffusivity, $C_p$ is the specific heat and $\rho_V$ is the density measured by the Archimedean principle as previously mentioned. Specific heat measurements (DSC 403 F3, Netzsch) were performed by the continuous scanning method under argon atmosphere.

## 3. Results and discussion

### 3.1 Glass-ceramics formation and microstructure

The crystallization behavior of the $Cu_{15}As_{30}Te_{55}$ glass was investigated using DSC experiments. The thermograms presented in Figure 1a show the evolution of thermodynamic properties up to 573K using different heating rates (ν = 5, 10, 20 and 40K.min$^{-1}$). Two characteristic temperatures are clearly observed on the DSC curves: the glass transition temperature $T_g$ and the crystallization temperature $T_p$. Both temperatures increase with the heating rate. Increasing the heating rate from 5K.min$^{-1}$ to 40K.min$^{-1}$, $T_g$ and the first crystallization temperature $T_{p1}$ shift from 394K to 408K and from 423K to 441K, respectively. According to Hruby,[15] the difference between these two temperatures ($T_{p1} - T_g$) can be used as a criterion to determine the thermal stability of a glass which is considered as stable when this difference exceeds 100K. In the present case, a difference of ~30K is obtained indicating that this glass is rather thermally unstable. The presence of two distinct exothermic peaks suggests that the crystallization of two different phases occurs. The peaks are better resolved at low heating rates *i.e.* at 5 or 10K.min$^{-1}$. The crystallization activation energy $E_c$ can be inferred using the method introduced by Ozawa and specifically designed for non-isothermal study.[16] As shown in Figure 1b, the value of $E_c$ is deduced from the slope of $\ln\nu$ plotted as a function of $1000/T_{p1}$ following the relation

$$\frac{d(\ln\nu)}{d\left(\frac{1}{T_{p1}}\right)} = -\frac{E_c}{R} \qquad (2)$$

where $R$ is the gas constant. The crystallization energy $E_c$ of the first peak $T_{p1}$ is equal to 189 kJ.mol$^{-1}$. This low value suggests that the glass composition requires few amount of energy to jump to crystalline state hence, making the sample poorly stable and quite prone to crystallization.

The SPS parameters (pressure, temperature, vertical displacement of punches) during the sintering process are shown in Figure 2. The sintering process starts around 373K to become maximal at 413K before ending at 423K. It is generally assumed that the sintering of amorphous powders by SPS proceeds through a viscous flow mechanism.[17] For the synthesis of glass-ceramics, two mechanisms have been assumed. The first one associates the densification of glassy powder through viscous sintering to a subsequent devitrification of the matrix.[17] The second possible mechanism implies densification and concomitantly a gradual crystallization of the matrix through the growth of neck between glassy particles.[17] For a given glass composition, the amorphous phase has a considerably lower viscosity than the corresponding crystalline phase, so that the sintering of polycrystalline material is inevitably more difficult than its amorphous counterpart. This suggests that the first mechanism described above, *i.e.* achieving full density prior to any significant crystallization, is likely at play. Moreover, it is well known that the current distribution in the SPS die and through the sample is different in the case of a conductor and an insulating material.[18] In the case of a non-electrically conducting sample such as alumina or silica based glass, no Joule heating is expected through the sample so that the die ensures sample's heating. This contrasts with the case of conducting materials such as metals or metallic glasses, for which Joule heating starts immediately through the sample at the beginning of the process. Due to the semiconducting properties of the $Cu_{15}As_{30}Te_{55}$ glass composition,[19] we surmise that heating occurs through both the carbon die and the powder.

Based on the above considerations, a series of SPS experiments was carried out in order to obtain either a glass bulk material or glass-ceramics with different crystalline fractions. From the DSC data collected at the rate of 40K.min$^{-1}$, the sintering temperatures were chosen accordingly to lie between the glass transition and the first crystallization temperature *i.e.* 423K or 433K. Applied pressures of 50 and 100MPa were selected and different dwell times were tested (0, 2, 5, 10 and 30 min.) with the aim of varying the crystalline fraction.

The density of the glass bulk material was measured to be 5.9 g.cm$^{-3}$ when the conditions 100MPa-423K-no-dwell-time were applied (Table 1). This value compares well with that obtained on the initial glass synthesized by the conventional melt-quenching technique. The PXRD pattern of the obtained pellet was indeed that of an amorphous material (Figure 3b) demonstrating that fully-densified amorphous samples were successfully obtained by SPS treatment. Upon partial crystallization, the density increases to 6.30 ± 0.10 g.cm$^{-3}$ at the maximum crystalline fraction (433K, 50MPa, 2' dwell time). As we shall see below, this result can be attributed to the crystallization of the β-$As_2Te_3$ compound that has a theoretical density of 6.29 g.cm$^{-3}$.[20]

PXRD measurements were carried out to determine the nature of the phases crystallizing in the glassy matrix (Figures 3c to 3h). The well-defined peaks showing up correspond to the crystallization of the β-$As_2Te_3$ phase (see Figure 3a for its PXRD pattern). An additional small peak appearing at longer dwell time (marked by *) could not be unambiguously identified and might correspond to either α-$As_2Te_3$, AsTe or CuTe.

Figures 4a to 4c show the EDXS measurements performed to obtain further information on the microstructure and its evolution with the SPS parameters. In the present case, a precise determination of the crystalline fraction is challenging given the different phases coexisting at the micron and sub-micron scales *i.e.* an amorphous phase containing well-crystallized nano-sized precipitates surrounded by biphasic regions composed of dendritic crystalline domains

embedded in a glassy matrix. Thus, as a first estimation, only the relative part of each domain (amorphous and biphasic) was determined using image-analysis software on EDXS-SEM pictures. The percentage obtained should therefore be regarded as an upper bound of the actual crystalline fraction. Within this rough approximation, the results indicate an increase in the crystalline fraction as the dwell time increases up to 30 min. under the same temperature and pressure conditions (Table I). EDXS reveals that Te and As elements are homogeneously distributed in the material which is not the case for the Cu (Figure 5). Quantitative analyses of these crystals suggest that the chemical composition corresponds to $As_2Te_3$ without any detectable traces of Cu, further corroborating the indexation of the PXRD pattern. As a consequence, the remaining glassy domains are enriched in Cu compared to the composition of the initial amorphous phase. Based on these images, the crystallized nano-sized domains are estimated to be less than 100 nm.

More intriguing is the fact that the β-form of $As_2Te_3$ crystallizes in the present case. While α-$As_2Te_3$ (monoclinic structure, space group $C2/m$)[20] is stable in ambient conditions and can be easily synthesized by conventional solid-state synthesis routes, the β-$As_2Te_3$ allotropic structure (rhombohedral structure of $Bi_2Te_3$ structure type, space group $R\bar{3}m$)[20-22] is metastable and could be so far only synthesized under high-pressure or by rapid quenching.[20-23] The fact that the metastable high-pressure β-$As_2Te_3$ phase is favored in the glass may be due to the constraint of the material through an applied pressure during the SPS process. It's well known that the β variety is denser than the stable α form.[23] Thus a phase transition $\beta \rightarrow \alpha$ at room temperature would imply an increase in volume $\Delta V_{\beta\rightarrow\alpha} > 0$.[23] Since the β-$As_2Te_3$ crystals are embedded in the glassy matrix, this volume change is prevented in the present case.

This conclusion seems to be further corroborated by neutron thermodiffraction experiments carried out to determine not only the nature of the phase crystallizing in the

glassy matrix but also their evolution upon heating. Figures 6a and 6b show 3D plots of the entire set of data collected up to 473K on the $Cu_{15}As_{30}Te_{55}$ and $Cu_{20}As_{20}Te_{60}$ glasses, respectively. Up to 405K, both samples remain in an amorphous state without any discernable changes. Above this temperature, three distinct peaks are visible at 48.1°, 65.5° and 75.5° (Figures 7a to 7c) and correspond to the three main reflections of the β-$As_2Te_3$ phase. Within a very narrow temperature window of ~2K, the β-$As_2Te_3$ phase undergoes a structural transition to the α-type structure that does not show further evolution with temperature up to 473K. These results clearly indicate a narrow domain of existence of the β-$As_2Te_3$ phase and show that, at temperatures at which the SPS treatment is performed (423 and 433K), the α-$As_2Te_3$ phase should be predominant in the crystalline fraction of the composite sample. The applied pressure during the SPS process together with internal stresses thus likely plays an important role in the stabilization of the β phase.[23]

Upon closer inspection of Figure 3 (patterns h and g), it can be noticed that, even in the most crystallized sample, the reflections corresponding to β-$As_2Te_3$ in the PXRD pattern are broad likely due to the size of the precipitates and/or microstrains. To determine which mechanism is at play here, the integral breadth of the reflections was evaluated based on PXRD data at higher resolution collected on the most-crystallized sample (Figure 8). The so-called Williamson–Hall relation then allows separating the size ($D_v$, volume-weighted column length) from the microstrain ($\varepsilon$, maximum strain) broadening.[24] These two quantities are related to the intrinsic integral breadth by:

$$\frac{\beta_e \cos\theta}{\lambda} = \frac{4\varepsilon \sin\theta}{\lambda} + \frac{1}{D_v} \qquad (3)$$

where λ is the wavelength of the CuKα radiation. As shown in Figure 9, $\frac{\beta_e \cos\theta}{\lambda}$ clearly varies linearly with the scattering vector $\frac{2\sin\theta}{\lambda}$. A linear fit against the experimental data

with $D_v$ and $\varepsilon$ as fitting parameters yield $D_v$ = 80 ± 30 nm and $\varepsilon$ = 0.29% ± 0.06%. A better estimation of both $D_v$ and $\varepsilon$ was derived from Rietveld refinements of the pattern using the Fullprof software.[25] This method enables a more reliable analysis of the microstructural effects by fitting each reflection to a pseudo-Voigt function, unlike the Williamson–Hall plot where a Lorentzian profile is assumed. In the literature, two $Bi_2Te_3$-type structures were reported for β-$As_2Te_3$ by Shu et al.[21,22]. These two models differ by slightly different positions of the As and Te atoms. We initially refined the experimental data considering both structures. In each case, the positions of the atoms and the lattice parameters were kept constant and the size and strain parameters were solely allowed to vary. Since a better agreement was found with the structure reported by Shu et al.[22] in 1986 (R-factors of $R_B$ = 21.5% and $R_B$ = 31.3%, respectively), refinements were pursued with this structure. In a second step, the positions of the atoms were released. The best refinement (Figure 8) led to $D_v$ = 73 nm and $\varepsilon$ = 0.28% (R-factors of $R_p$ = 0.9% and $R_B$ = 13.7%). As a consistency check, the same analysis was repeated in another part of the sample and yielded very similar values ($D_v$ = 82 nm and $\varepsilon$ = 0.39%). While the size of the crystalline domain of metastable β-$As_2Te_3$ – found to be small – is consistent with EDXS analyses, the value of the strain parameter is more surprising. Such high value, similar to that found in ball-milled molybdenum (0.4%) for instance,[26] may be considered as evidence of the presence of strong internal stresses stabilizing the β form of the $As_2Te_3$ compound.

### 3.2 Thermoelectric properties

Figure 10 shows the temperature dependence of the electrical resistivity of the glass and glass-ceramic samples. The ρ values of the amorphous parent compound reach about 1 Ω.m at 300K, in line with previous results.[19] The electrical resistivity decreases by 4 orders of magnitude when crystals of β-$As_2Te_3$ are present in the glassy matrix. This decrease mainly

originates from the presence of crystalline phase rather than an enhancement of the copper enriched amorphous phase since the decrease is almost doubled to that observed in pure As-Te-Cu glasses with different Cu contents.[27] As mentioned above, $As_2Te_3$ crystallizes in two allotropic forms consisting of either a rhombohedral structure (β-$As_2Te_3$) or a monoclinic structure (α-$As_2Te_3$). α-$As_2Te_3$ exhibits at 300K high thermoelectric power (ranging between -230 and -260 μV/K), low thermal conductivity (estimated to 4.0 $W.m^{-1}.K^{-1}$) and an electrical resistivity value of 40 μΩ.m.[20,28] Though the thermopower values of β-$As_2Te_3$ remains so far unknown, it might show similar α values due to the strong similarities in the crystal and electronic structures of both compounds.[29]

Regardless of the crystalline fraction, α slowly increases with temperature up to 365K and shows positive values indicating that all the samples are *p*-type materials (Figure 11). The $Cu_{15}As_{30}Te_{55}$ parent glass exhibits the highest α value reaching 900$\mu V.K^{-1}$ at 315K. The presence of crystalline β-$As_2Te_3$ in the glassy matrix markedly influences the values of α that drop to 70$\mu V.K^{-1}$ at the maximum crystalline fraction. While the strong decrease in the ρ values may be the main ingredient lowering α as usually observed in crystalline semiconductors, the type of charge carriers dominating the electronic transport in β-$As_2Te_3$ may also play a significant role. When both electrons and holes contribute to the electrical conduction, α decreases due to the opposite sign of the contribution to the thermopower of both carriers. In the present case, if β-$As_2Te_3$ indeed behaves as an *n*-type semiconductor as suggested by Scheidemantel et al.[20], its contribution to α would then partially cancel that of the amorphous phase thereby decreasing the overall α values.

To further investigate this last possibility, thermopower mapping of the surface of glass-ceramic compounds was carried out. Figure 12a shows a map realized on a 4×0.5 $mm^2$ surface area on the glass-ceramics obtained with the SPS parameters 423K, 100MPa and 30 min. for which, both amorphous and biphasic phases coexist (Figure 12b). The distribution of

the thermopower values, depicted in Figure 12c, clearly indicates contributions from two distinct phases: one coming from a phase with high positive α values and a second with lower α values. The observed two-peak structure of the recorded signal may thus correspond to the amorphous and crystalline domains, respectively. Considering the average effect of the thermopower mapping due to the presence of dendritic domains of size below the resolution of the instrument, the tendency of the low α values towards negative values might indicate an intrinsic *n*-type behavior of the β-$As_2Te_3$ crystals.

The presence of a substantial crystalline fraction in the glassy matrix does not lead to drastic changes in specific heat $C_p$ that amounts to 0.25 $J.g^{-1}.K^{-1}$ at 300K regardless of the crystalline fraction. The thermal conductivity values, listed in Table I, clearly increase concomitantly with the crystalline fraction: on going from the pure amorphous phase to the most crystallized sample, $\lambda$ increases from 0.2 to 1.1 $W.m^{-1}.K^{-1}$ at 300K. This change towards higher values cast doubt on the validity of the assumption made in Ref. 30 where a value measured in the $Ge_{20}Te_{80}$ glassy material has been used to estimate the *ZT* value of the Cu-containing samples (glass and glass-ceramics samples). The actual *ZT* value is likely to be significantly lower than the estimation given (0.2 at 300K). Note that such a trend with the crystalline fraction is not confined to the present glass-ceramics and has been already observed in oxide glass-ceramics.[21]

These results provide an alternative way to estimate the crystalline fraction in the glass-ceramic samples. Within the effective-medium approach developed by Landauer[31] to model the thermal conductivity of composite materials, the thermal conductivity of the glass-ceramic samples composed of crystallized and amorphous phases can be expressed as

$$\lambda_{crys} = \frac{2\lambda_{exp}{}^2 - \lambda_{exp}\lambda_{glass}(3f_{glass} - 1)}{\lambda_{glass} + \lambda_{exp}(3f_{crys} - 1)} \quad (4)$$

where $\lambda_{crys}$ is the thermal conductivity of the β-$As_2Te_3$ phase, $\lambda_{glass}$ is the thermal conductivity of the pure amorphous compound, $f_{glass}$ is the volume fraction of the amorphous phase and $f_{crys} = 1 - f_{glass}$ is the volume fraction of the crystallized phase. Assuming that the thermal conductivity of β-$As_2Te_3$ is $\lambda_{crys}$ = 4.0 $W.m^{-1}.K^{-1}$ and using the experimental values of $\lambda_{crys/glass}$ and $\lambda_{glass}$, the volume fraction of the crystallized phase $f_{crys}$ may be inferred.[29] The values obtained by this model, and listed in Table I, indicate a rather non-linear increase in the crystalline fraction when the dwell time increases. At the longest dwell time used here corresponds the maximum crystalline fraction that amounts to ~ 43%.

The highest power factor ($P \approx$ 260 $\mu W.K^{-2}.m^{-1}$ at $T =$ 300K) was achieved in the glass-ceramics exhibiting the highest crystalline fraction. Combined with the thermal conductivity values, this leads to a *ZT* value of ~ 0.08 at 300K that increases to 0.14 at 365K. This value remains low compared to that of $Bi_2Te_3$-based materials considered as reference materials for room temperature applications. This limitation in the *ZT* enhancement may result from the balance between the positive influence of crystallized β-$As_2Te_3$ on the electrical resistivity and its detrimental effect on the thermopower. Further optimization of the thermoelectric performance might be achieved provided *p*-type crystals in an intrinsically *p*-type glassy matrix could be grown.

## 4. Conclusion

The microstructure and thermal stability of the $Cu_{15}As_{30}Te_{55}$ glass and its corresponding glass-ceramics analogues were investigated by means of DSC, x-ray diffraction and temperature-dependent neutron diffraction experiments. Transport properties measurements were further carried out to determine the influence of a partial crystallization on the thermoelectric properties. SPS-controlled process was demonstrated to be an efficient tool to

crystallize a substantial fraction of the glassy matrix. The metastable β-$As_2Te_3$ phase was found to crystallize first through the glassy matrix as the dwell time or the temperature of the SPS treatment increases. While this phase should undergo a transition to the stable α-$As_2Te_3$ above 409K *i.e.* at temperatures below that of the SPS treatment, the metastable β phase is found to be solely present in the glass-ceramics samples regardless of the SPS parameters used. The applied pressure and/or internal stresses during crystal growth likely play a role in the stabilization of this phase. The presence of crystallized domains has a strong and beneficial influence on the electrical resistivity that decreases by four orders of magnitude. This result provides a proof-of-principle showing the potential of this approach in tuning the electrical conduction in chalcogenide-based glasses. Yet, our study also suggests that the nature of the crystalline phase is essential in optimizing the thermoelectric efficiency. In the present case, the crystallization of β-$As_2Te_3$ lowers the thermopower values possibly due to an intrinsic *n*-type behavior suggested by thermopower mapping. The *ZT* values are nevertheless enhanced in the glass-ceramic samples reaching 0.14 at 365K. The control of the type of conduction of the crystalline phase appears crucial to improve the thermoelectric efficiency of glass-ceramic compounds. This may be realized via changing and/or doping the initial glass composition and will be at the core of forthcoming studies.

**Acknowledgements**

The authors would like to thank financial support from the French National Agency (ANR) in the frame of its programme "PROGELEC" (Verre Thermo-Générateur “VTG”). G. D. also acknowledges the support from the Limousin Region for its financial support through FEDER program. E. B. L. and A. P. G. acknowledge the support of FCT, Portugal under the contract nr. PTDC/CTM/102766/2008.

## References


1 A. F. Ioffe, in *Semiconductor Thermoelements and Thermoelectric Cooling*, Infosearch, London, 1957.

2 G. J. Snyder and E. S. Toberer, *Nature Materials*, 2008, **7**, 105.

3 D. M. Rowe, in *Thermoelectrics Handbook: Macro to Nano*, CRC/ Taylor & Francis, Boca Raton, FL, 2006.

4 K. Biswas, J. He, I. D. Blum, C.-I. Wu, T. P. Hogan, D. N. Seidman, V. P. Dravid and M. G. Kanatzidis, *Nature*, 2012, **489**, 414.

5 J. He, J. Androulakis, M. G. Kanatzidis and V. P. Dravid, *Nano Lett.*, 2012, **12**, 343.

6 Y. Pei, N. A. Heinz, A. LaLonde and G. J. Snyder, *Energy Environ. Sci.*, 2011, **4**, 3640.

7 Y. Pei, J. Lensch-Falk, E. S. Toberer, D. L. Medlin and G. J. Snyder, *Adv. Funct. Mater.*, 2011, **21**, 241.

8 O. Bubnova, Z. Ullah Khan, A. Malti, S. Braun, M. Fahlman, M. Berggren, X. Crispin, *Nature Mater.*, 2011, 10, 429.

9 K. C. See, J. P. Feser, C. E. Chen, A. Majumdar, J. J. Urban, R. A. Segalman, *Nanoletters*, 2010, 10, 4664.

10 M. He, J. Ge, Z. Lin, X. Feng, X. Wang, H. Lu, Y. Yang, F. Qiu, *Energy Environ. Sci.*, 2012, 5, 8351.

11 D. Souri*, J. Phys. D: Appl. Phys.*, 2008, **41**, 105102.

12 L.J. Van der Pauw, *Philips Research Reports*, 1958, **13**, 1.

13 R. T. Littleton IV, J. Jeffries, M. Kaeser, M. Long, and T. M. Tritt, *Mater. Res. Soc. Symp. Proc.*, 1999, **545**, 137.

14 D. Platzek, G. Karpinski, C. Stiewe, P. Ziolkowski, C. Drasar, and E. Müller, in *Proceedings of the 24th International Conference on Thermoelectrics*, IEEE, New York, p. 13, 2005.

15 A. Hruby, *Czech J. Phys.*, 1972, **B22**, 1187.

16 T. Ozawa, *Polymer*, 1971, **12**, 150.

17 M. N. Rahaman, in *Sintering of ceramics*, p.47, CRC/Taylor and Francis, 2008.

18 U. Anselmi-Tamburini, S. Gennari, J.E. Garay and Z.A. Munir, *Materials Science and Engineering A*, 2005, **394**, 139.

19 E. Marquez, J. Vazquez, N. de la Rosa-Fox, P. Villares and R. Jimenez-Garay, *J. Mater. Sci.*, 1988, **23**, 1399.

20 T. J. Scheidemantel, J. F. Meng and J. V. Badding, *Journal of Physics and Chemistry of Solids*, 2005, **66**, 1744.

21 H.W. Shu, S. Jaulmes and J. Flahaut, *Journal of Solid State Chemistry*, 1988, **74**, 277.

22 H. W. Shu, S. Jaulmes and J. Flahaut, *Materials Research Bulletin*, 1986, **21**, 1509.

23 S. Toscani, J. Dugue, R. Ollitrault and R. Ceolin, *Thermochimica Acta*, 1991, **186**, 247.

24 G.K. Williamson and W.H. Hall, *Acta Metallurgica*, 1953, **1**, 22.

25 J. Rodriguez-Carvajal, *Physica B*, 1993, **192**, 55.

26 I. Lucks, P. Lamparter and E.J. Mittemeijer, *J. Appl. Cryst.*, 2004, **37**, 300.

27 A. P. Gonçalves, E. B. Lopes, G. Delaizir, J. B. Vaney, B. Lenoir, A. Piarristeguy, A. Pradel, J. Monnier, P. Ochin, C. Godart, *J. Sol. State Chem.*, 2012, **193**, 26.

28 T. C. Harman, B. Paris, E. Miller and H. L. Goering, *J. Phys. Chem. Solids*, 1957, **2**, 181.

29 T. J. Scheidemantel and V. Badding, *Solid State Commun.*, 2003, **127**, 667.

30 A. P. Gonçalves, E. B. Lopes, O. Rouleau and C. Godart, *J. Mater. Chem.*, 2010, **20**, 1516.

31 R. Landauer, *J. Appl. Phys.*, 1952, **23**, 779.

Table I. Density, volume fraction of the biphasic domains, room temperature thermoelectric properties and crystalline fraction inferred from Eq.(4) of the different SPS glasses and glass-ceramics.

| *SPS parameters* | *0'-423K-100MPa* | *5'-423K-100MPa* | *10'-423K-100MPa* | *30'-423K-100MPa* | *2'-433K-50MPa* |
|---|---|---|---|---|---|
| Density ($g.cm^{-3}$) | 5.90 ± 0.1 | 6.03 ± 0.1 | 6.13 ± 0.1 | 6.23 ± 0.1 | 6.30 ± 0.1 |
| Biphasic fraction (vol %) | 0 | 53 | 67 | 80 | 89 |
| ρ (mΩ.cm) | $7.9.10^4$ | 8.2 | 7.2 | 4.3 | 1.2 |
| α ($\mu V.K^{-1}$) | 870 | 70 | 72 | 69 | 55 |
| Power factor ($\mu W.m^{-1}.K^{-2}$) | 1 | 60 | 72 | 111 | 257 |
| λ ($W.m^{-1}.K^{-1}$) | 0.22 | 0.40 | 0.43 | 0.50 | 1.07 |
| $f_{crys}$ (vol %) | 0 | 18 | 21 | 25 | 43 |
| ZT (300K) | 0.001 | 0.004 | 0.050 | 0.060 | 0.072 |

## Figure captions

Figure 1: (a) DSC curve of the $Cu_{15}As_{30}Te_{55}$ glass, (b) calculation of crystallization energy $E_c$ by Ozawa's method.

Figure 2: Graph showing the pressure applied and shrinkage (in mm) as a function of temperature during SPS sintering of the $Cu_{15}As_{30}Te_{55}$ glassy powder.

Figure 3: XRD patterns of (a) β-$As_2Te_3$, glass and glass-ceramics sintered with the SPS parameters (b) 423K, 100MPa, 0 min., (c) 423K, 100MPa, 1 min., (d) 423K, 100MPa, 3 min. (e) 423K, 100MPa, 5 min., (f) 423K, 100MPa, 10 min., (g) 423K, 100MPa, 30 min., (h) 433K, 50MPa, 2 min.

Figure 4: SEM images of SPS glass and glass-ceramics showing the presence of dendritic crystallized structures in the glassy matrix for (a) 423K, 100MPa, 10 min., (b) 423K, 100MPa, 30 min., (c) 433K, 50MPa, 2 min.

Figure 5: Composition measured by EDXS revealing the presence of β-$As_2Te_3$ surrounded by a Cu-rich glassy matrix.

Figure 6: 3D plots of the powder thermodiffraction data collected between 10° and 120° as a function of temperature for the (a) $Cu_{15}As_{30}Te_{55}$ and (b) $Cu_{20}As_{20}Te_{60}$ samples.

Figure 7: (a) 2D mapping of the diffraction data of the $Cu_{20}As_{20}Te_{60}$ sample as a function of temperature showing the transition from the β-$As_2Te_3$ to the α-type structure that occurs near 409 K. (b) Magnification of the neutron thermodiffraction data near the β-α phase transition. The main reflections of the β and α phases are marked by a white circle and a black square, respectively. (c) Neutron powder diffraction pattern highlighting the structural transition that sets in between 405 and 409K.

Figure 8: Rietveld refinement of the high-resolution x-ray powder pattern (see text for explanations) of the sample labeled (h) in Fig. 3. The open circles are the experimental data, the line is the calculated pattern, the bottom line is the difference pattern (exp. – calc.) and the upper ticks are the Bragg angles corresponding to β-$As_2Te_3$. The main reflection of the second phase is labeled by a star.

Figure 9: Williamson – Hall plot of the sample integral breadth ($\beta_e$) as a function of the scattering vector length. The solid squares stand for the experimental data while the solid black line is the best to the data according to Eq.(2).

Figure 10: Electrical resistivity as a function of temperature for different SPS glass and glass-ceramics samples.

Figure 11: Thermopower as a function of temperature for different glass and glass-ceramic samples.

Figure 12: (a) Mapping of the Seebeck coefficient ($4\times0.5mm^2$) of the glass-ceramics (423K, 100MPa, 30 min.), (b) Corresponding SEM photograph with chemical contrast (BSE) between glassy phase (dark grey) and crystalline phase (light grey), (c) Distribution of thermoelectric power values on the whole cartography (a).

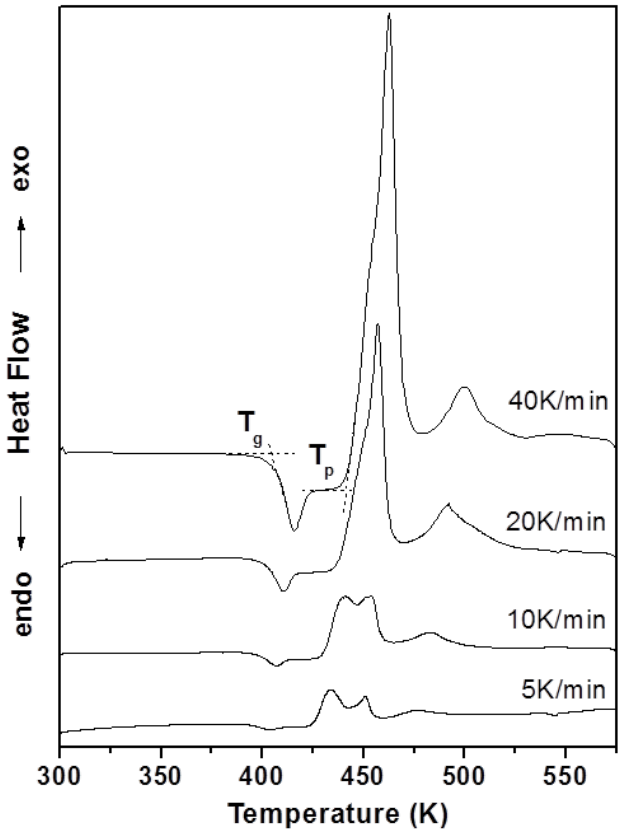
exo
Heat Flow
endo
T
g
T
p
40K/min
20K/min
10K/min
5K/min
300
350
400
450
500
550
Temperature (K)

**Figure 1**

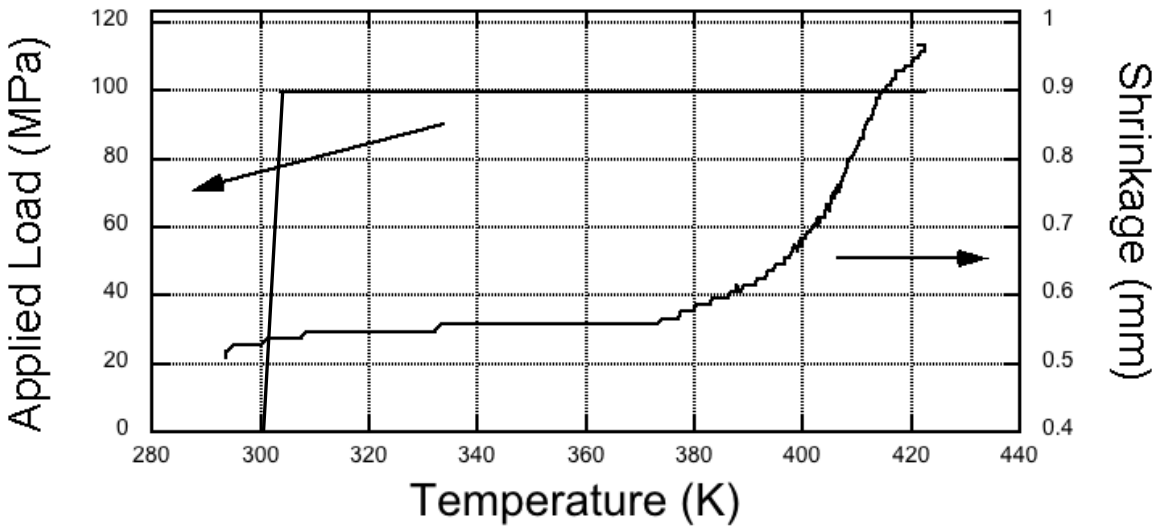
Applied Load (MPa)
Shrinkage (mm)
Temperature (K)
120
100
80
60
40
20
0
1
0.9
0.8
0.7
0.6
0.5
0.4
280
300
320
340
360
380
400
420
440

**Figure 2**

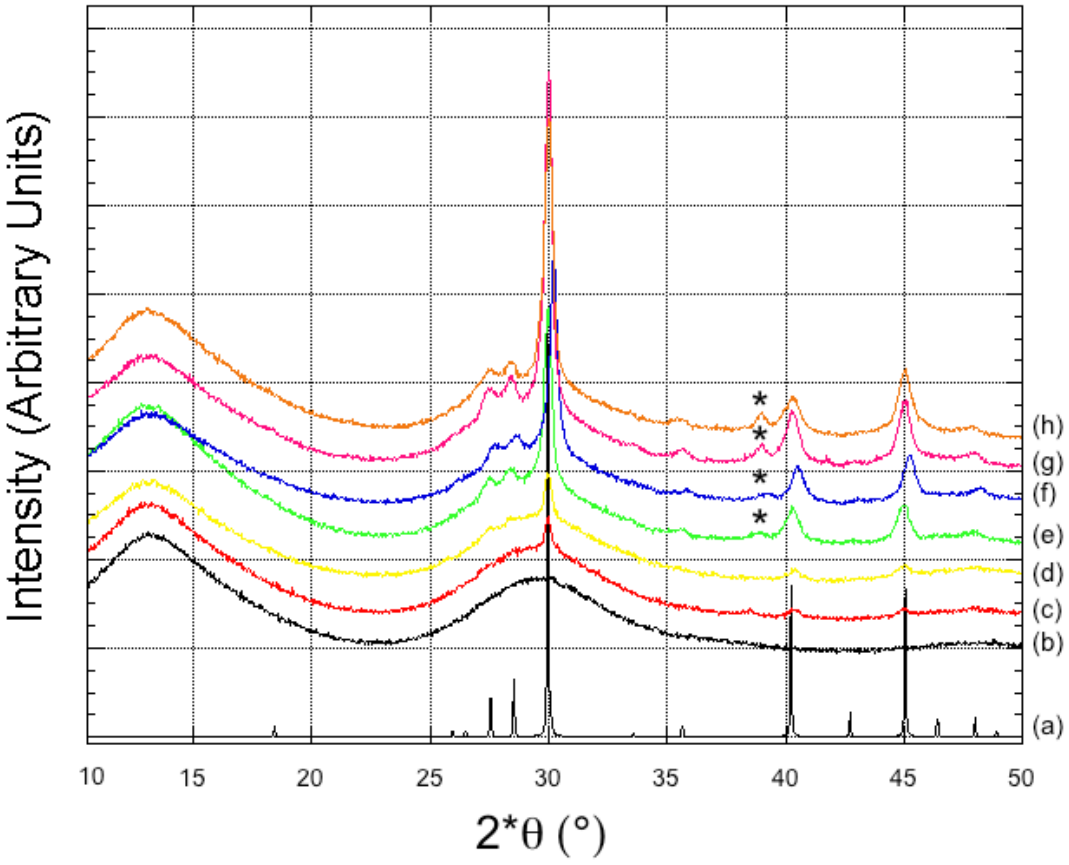
Intensity (Arbitrary Units)
2*θ (°)
10
15
20
25
30
35
40
45
50
(h)
(g)
(f)
(e)
(d)
(c)
(b)
(a)
*
*
*
*

**Figure 3**

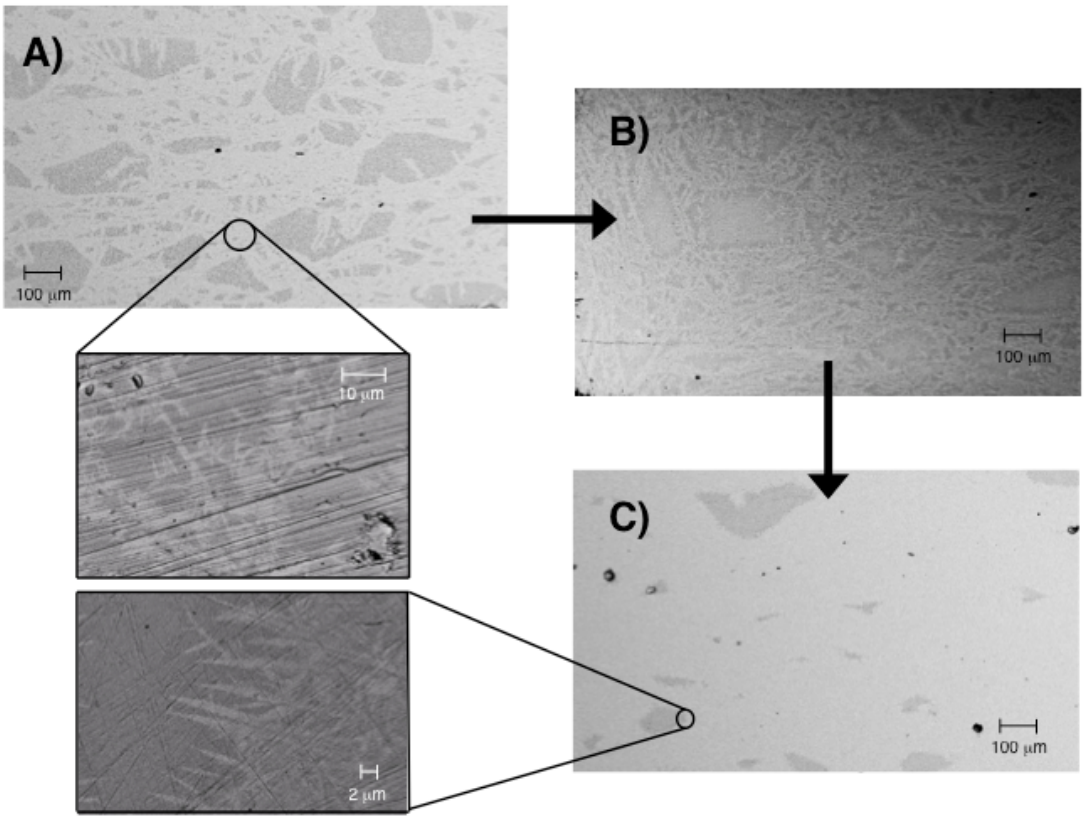


**Figure 4**

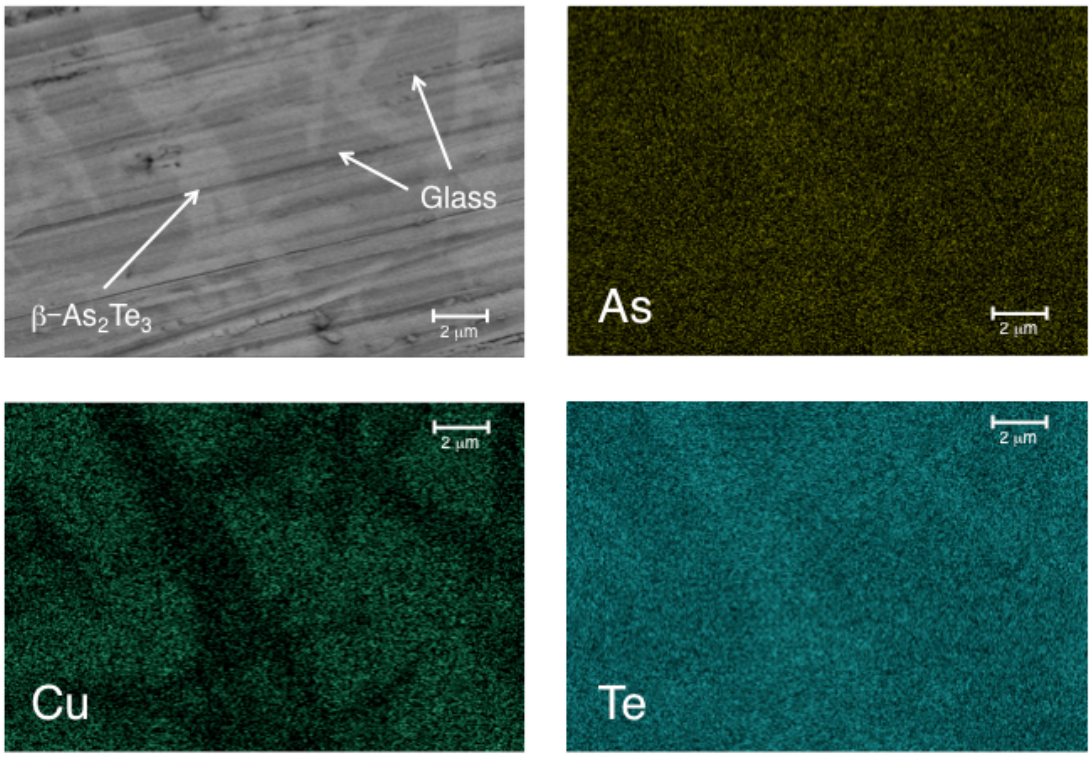


**Figure 5**

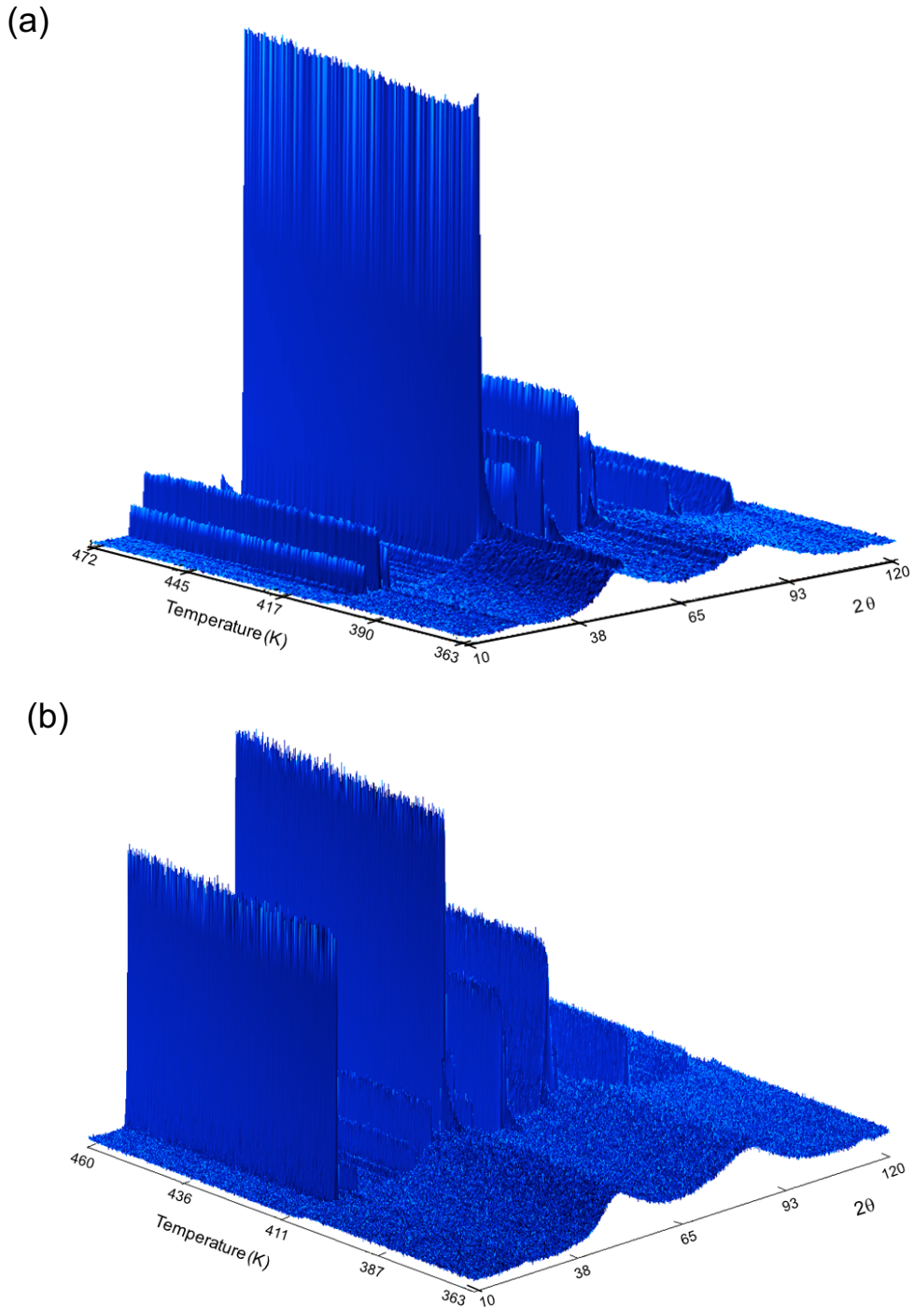
(a)
472
445
417
390
363
Temperature (K)
10
38
65
93
120
2θ
(b)
460
436
411
387
363
Temperature (K)
10
38
65
93
120
2θ

**Figure 6**

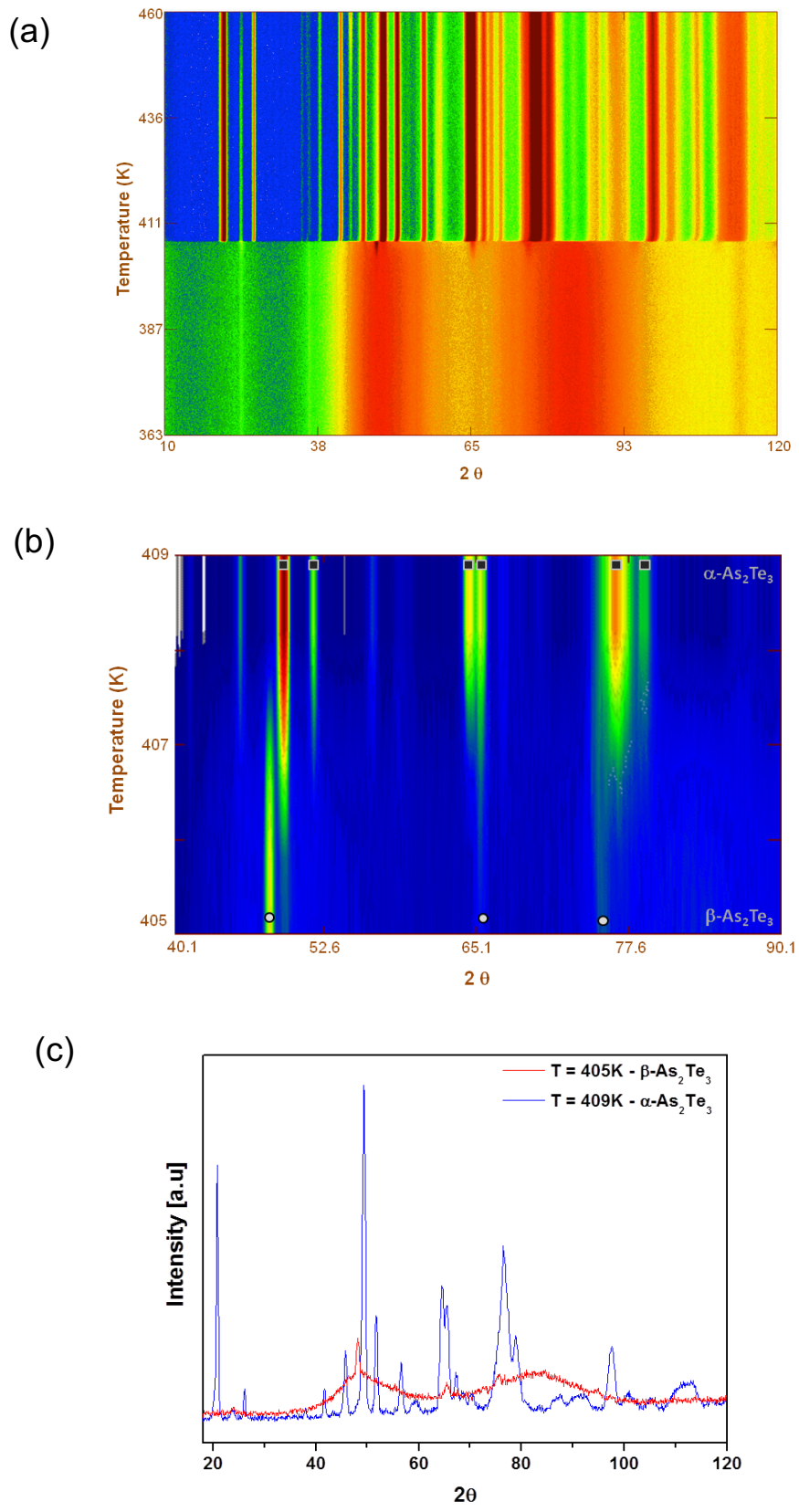
(a)
460
436
411
387
363
Temperature (K)
10
38
65
93
120
2 θ
(b)
409
407
405
Temperature (K)
α-As2Te3
β-As2Te3
40.1
52.6
65.1
77.6
90.1
2 θ
(c)
T = 405K - β-As2Te3
T = 409K - α-As2Te3
Intensity [a.u]
20
40
60
80
100
120
2θ

**Figure 7**

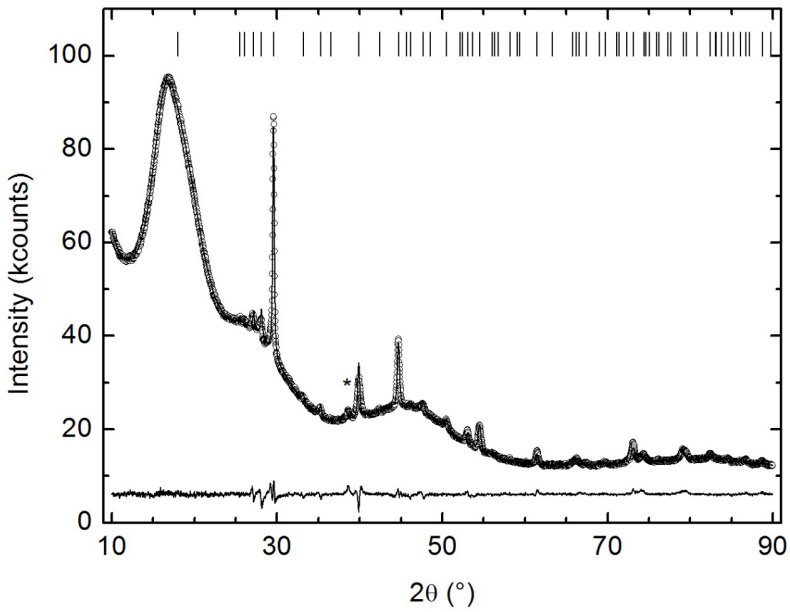


**Figure 8**

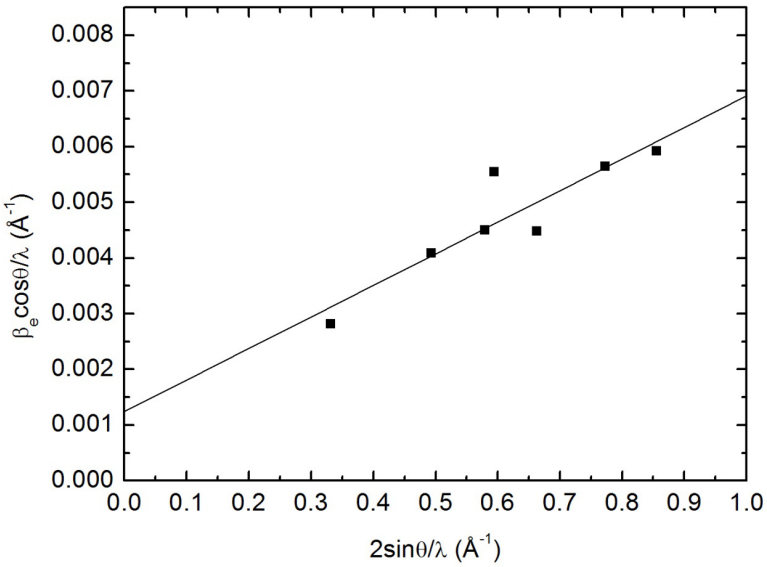
0.008
0.007
0.006
0.005
0.004
0.003
0.002
0.001
0.000
$\beta_e \cos\theta/\lambda$ (Å$^{-1}$)
0.0 0.1 0.2 0.3 0.4 0.5 0.6 0.7 0.8 0.9 1.0
$2\sin\theta/\lambda$ (Å$^{-1}$)

**Figure 9**

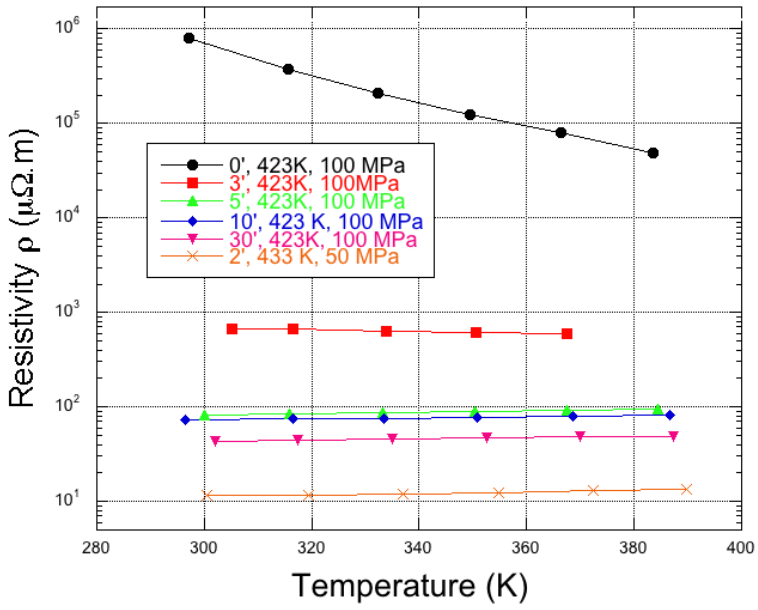
Resistivity ρ (μΩ.m)
Temperature (K)
0', 423K, 100 MPa
3', 423K, 100MPa
5', 423K, 100 MPa
10', 423 K, 100 MPa
30', 423K, 100 MPa
2', 433 K, 50 MPa

**Figure 10**

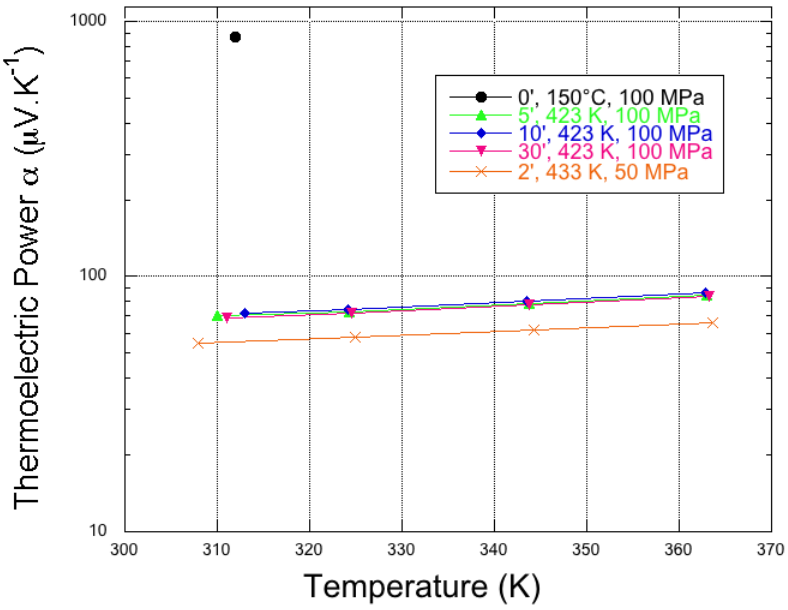
Thermoelectric Power α (μV.K-1)
1000
100
10
300
310
320
330
340
350
360
370
Temperature (K)
0', 150°C, 100 MPa
5', 423 K, 100 MPa
10', 423 K, 100 MPa
30', 423 K, 100 MPa
2', 433 K, 50 MPa

**Figure 11**

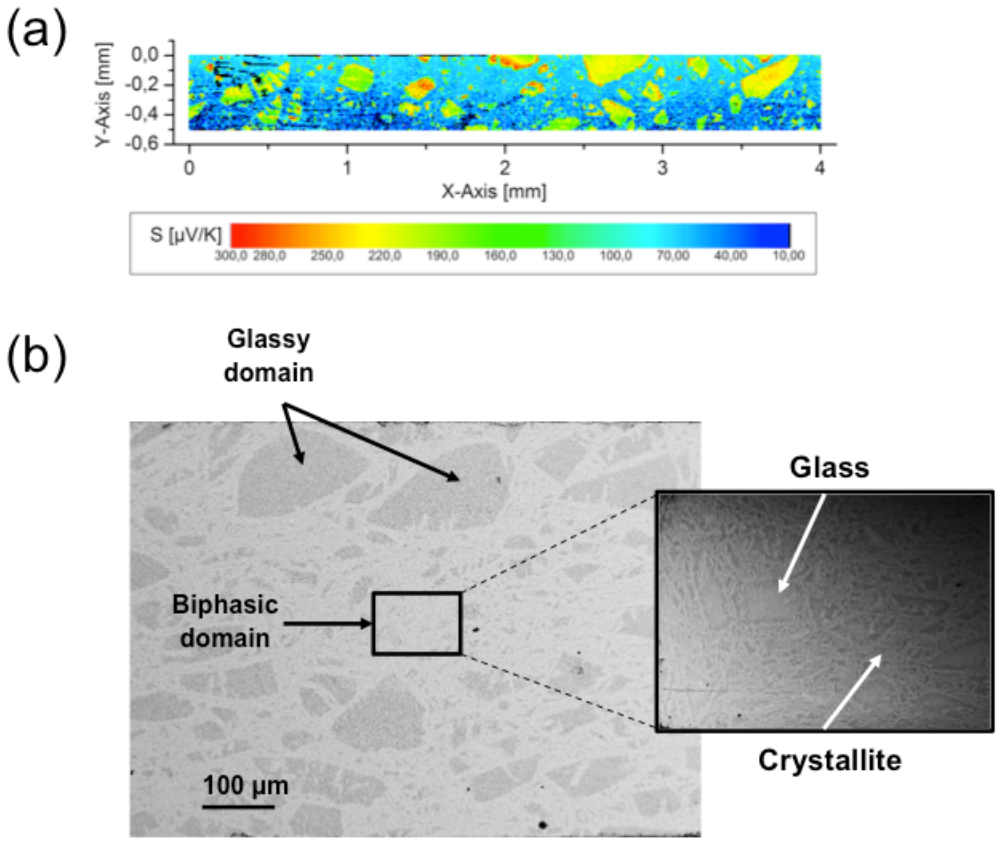
(a)
Y-Axis [mm]
0,0
-0,2
-0,4
-0,6
0
1
2
3
4
X-Axis [mm]
S [µV/K]
300,0 280,0 250,0 220,0 190,0 160,0 130,0 100,0 70,00 40,00 10,00
(b)
Glassy domain
Glass
Biphasic domain
Crystallite
100 µm
(c)
Counts
500
400
300
200
100
0
-50
0
50
100
150
200
250
300
Seebeckkoefficient [µV/K]

**Figure 12**